Inorg. Chem. **2006**, *45*, 547−554

Tuning the Electronic Communication and Rates of Intramolecular Electron Transfer of Dimers of Trinuclear Ruthenium Clusters: Bridging and Ancillary Ligand Effects

J. Catherine Salsman, Silvia Ronco,† Casey H. Londergan, and Clifford P. Kubiak*

Department of Chemistry and Biochemistry, University of California-San Diego, La Jolla, California 92093-0358

Received May 10, 2005

Ten new bridged dimers of oxo-centered triruthenium clusters with CO and 4-(dimethylamino)pyridine (dmap), pyridine (py), or 4-cyanopyridine (cpy) as terminal ligands and pyrazine-d_4 (d_4-pz), 2,5-dimethylpyrazine (dmpz), 2-methylpyrazine (mpz), and 2-chloropyrazine (clpz) as bridging ligands were prepared. The carbonyl stretching frequency, ν(CO), was used as a probe for infrared spectroelectrochemical measurements. In the neutral and doubly reduced states, a single band was observed for each of the dimers, with a shift in frequency due to the oxidation state of the triruthenium clusters. In the singly reduced state, a range of ν(CO) line shapes was observed, depending on the nature of the ligands, from two bands centered at the frequencies of the bands of the neutral and doubly reduced species to one broad band at the average of these two frequencies. By synthesizing new combinations of bridging and ancillary ligands, electronic communication between two bridged triruthenium clusters was effectively tuned, and electron-transfer rates were estimated by IR spectral line-shape analysis. In dimers bridged by the asymmetric ligand mpz, it was possible through selective isotope labeling of one CO ligand to observe "mixed-valence isomers," the two alternate charge distributions of a mixed-valence complex.

Introduction

Electron exchange dynamics in mixed-valence compounds have been the subject of extensive investigations.[1−3] Mixed-valence complexes have traditionally been categorized according to the Robin−Day classification scheme,[1] in which Class I complexes are charge-localized, Class II complexes are localized with electronic coupling between the metal centers, and Class III complexes are delocalized. It is often difficult to determine the precise threshold between Class II and Class III, and recently a fourth category, "borderline" Class II−III, was introduced.[3] Further, the term "delocalization" must be referenced to a time scale, and the actual rates of electron transfer in various Class II, Class III, and borderline mixed-valence complexes are seldom clearly known.

Previous work from this research laboratory showed that steady-state reflectance infrared spectroelectrochemical techniques can be used to study intramolecular electron-transfer processes in the picosecond time domain.[4−6] Hexaruthenium compounds of the type {[$Ru_3O(\mu\text{-}OAc)_6$](CO)(L)(μ-BL)-[$Ru_3O(\mu\text{-}OAc)_6$](CO)(L)}, where BL = bridging ligand (Figure 1), have been of interest because they display reversible multistep redox behavior.[4] Upon electrochemical reduction to form the mixed-valence state, infrared spectral line coalescence consistent with dynamic exchange on the vibrational time scale was observed by probing CO stretching frequencies, ν(CO). Ultrafast electron-transfer rate constants, k_{et}, were determined by analysis of the coalesced line shapes using an NMR-like Bloch equation analysis.[7,8]

Experimental evidence showed that it is possible to fine-tune the electronic coupling between the two cluster units

* To whom correspondence should be addressed. E-mail: ckubiak@ucsd.edu.

† On sabbatical leave from: Chemistry Department, University of South Dakota, SD 57069.

(1) Robin, M. B.; Day, P. *Adv. Inorg. Chem. Radiochem.* **1967**, *10*, 247−422.
(2) Allen, G. C.; Hush, N. *Prog. Inorg. Chem.* **1967**, *8*, 357−389.
(3) Demadis, K. D.; Hartshorn, C. M.; Meyer, T. J. *Chem. Rev.* **2001**, *101*, 2655−2685.
(4) Ito, T.; Hamaguchi, T.; Nagino, H.; Yamaguchi, T.; Washington, J.; and Kubiak, C. P. *Science* **1997**, *277*, 660−663.
(5) Ito, T.; Hamaguchi, H.; Nagino, H.; Yamaguchi, T.; Kido, H.; Zavarine, I. S.; Richmond, T.; Washington, J.; Kubiak, C. P. *J. Am. Chem. Soc.* **1999**, *121*, 4625−4632.
(6) Londergan, C. H.; Salsman, J. C.; Ronco, S.; Dolkas, L. M.; Kubiak, C. P. *J. Am. Chem. Soc.* **2002**, *124*, 6236−6237.
(7) Grevels, F. W.; Jacke, J.; Klotzbucher, W. E.; Kruger, C.; Seevogel, K.; Tsay, Y. H. *Angew. Chem., Int. Ed. Engl.* **1987**, *26*, 885−887.
(8) Grevels, F. W.; Kerpen, K.; Klotzbucher, W. E.; McClung, R. E. D.; Russell, G.; Viotte, M.; Schaffner, K. *J. Am. Chem. Soc.* **1998**, *120*, 10423−10433.

10.1021/ic050737v CCC: $33.50
Published on Web 12/15/2005

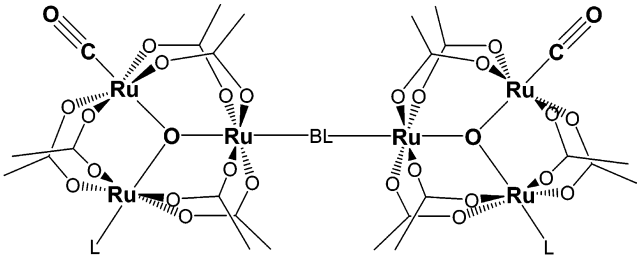

1: L= dmap; BL= pz
2: L= dmap; BL= d_4-pz
3: L= dmap; BL= mpz
4: L= dmap; BL= dmpz
5: L= py ; BL= pz
6: L= py; BL= d_4-pz
7: L= py; BL= mpz
8: L= py; BL= dmpz
9: L= py; BL= clpz
10: L= 4-cpy; BL= pz
11: L= 4-cpy; BL= d_4-pz
12: L= 4-cpy; BL= mpz
13: L= 4-cpy; BL= dmpz

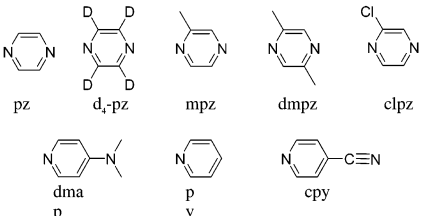

Figure 1. Structures of the triruthenium cluster dimers and the various bridging ligands.

by altering the nature of ancillary ligands, where L = pyridine (py), 4-cyanopyridine (cpy), or 4-(dimethylamino)-pyridine (dmap) and BL = pyrazine (pz).[4,5] The spectral line shapes range from less coalesced, or mixed-valence "trapped" (cpy), to highly coalesced, or dynamically averaged (dmap), depending on the relative electron-donor character of the ancillary ligands. This can be explained by considering that dπ(Ru) orbitals are raised to higher energies following the series cpy < py < dmap, allowing for a more efficient overlap with π*(BL) orbitals and resulting in more electronically delocalized states and, therefore, more highly coalesced spectra. Singly reduced species of dmap and py display Class III-like (delocalized) behavior according to the Robin−Day classification for mixed-valence complexes, whereas cpy complexes showed Class II behavior.[1] The electron-transfer rates were also found to be controlled by solvent dynamics, showing a strong correlation with solvent dipolar relaxation times.[6,9]

The interpretation of our earlier findings would suggest that electronic exchange between cluster units can also be manipulated by altering the nature of the bridging ligand. Spectroelectrochemical measurements for dimers containing 4,4′-bipyridine showed slower electron-transfer rates and uncoalesced infrared line shapes.[4,5] In this paper, we present our studies of the effects of introducing substituents on the pyrazine ring and, in particular, how this affects the electronic communication between clusters. We prepared three series of hexaruthenium clusters that contain pyrazine, deuterated pyrazine (d_4-pz), 2,5-dimethylpyrazine (dmpz), 2-methylpyrazine (mpz), and 2-chloropyrazine (clpz) as bridging ligands and pyridine (py), 4-cyanopyridine (cpy), and 4-(dimethylamino)pyridine (dmap) as ancillary ligands (Figure 1).

Experimental Section

Materials. All solvents for synthesis were obtained from Fisher and were used as received. For cyclic voltammetry, reflectance infrared spectroelectrochemistry, and electronic spectroscopy, solvents were dried over activated alumina. Tetra-*n*-butylammonium hexafluorophosphate (TBAH) was received from Aldrich and recrystallized from absolute ethanol and dried under vacuum at 100 °C for 24 h.

Preparation of Substituted Pyrazine-Bridged Dimers. The dimers were synthesized using the "metal complex as ligand" strategy previously described.[10] The syntheses of pz-linked dimers **1**, **5**, and **10** were reported previously.[4] Equimolar quantities of $Ru_3O(CH_3COO)_6(CO)(L)(BL)$ and $Ru_3O(CH_3COO)_6(CO)(L)(H_2O)$ were stirred in CH_2Cl_2 overnight. Purification procedures depended on solubility properties and the stabilities of the compounds. Individual modifications for each compound are described below.

1. $[Ru_3(\mu_3\text{-}O)(\mu\text{-}CH_3CO_2)_6(CO)(dmap)]_2(\mu\text{-}BL)$. (i) BL = Pyrazine-$d_4$, 2. $Ru_3O(CH_3COO)_6(CO)(dmap)(d_4\text{-pz})$ (300 mg, 0.339 mmol) and $Ru_3O(CH_3COO)_6(CO)(dmap)(H_2O)$ (286 mg, 0.339 mol) were dissolved in CH_2Cl_2 (50 mL) and stirred at RT overnight. The solvent was removed in vacuo, and the blue-green compound was chromatographed over silica gel (2% MeOH in CH_2Cl_2). The first blue-green (main) band was isolated and found to contain monomer and dimer. The solvent was again removed, and the dimer was separated from the monomer by gel filtration (Bio-Beads SX-3 in $CHCl_3$). The blue-green compound obtained after evaporation of the solvent was dissolved in a minimum amount of CH_2Cl_2 and precipitated with hexanes to give a dark blue-green powder (400 mg). Typical yield was 70%. Anal. calcd for $Ru_6C_{44}H_{56}D_4O_{28}N_6$: C, 31.10; H, 3.30; N, 4.95. Found: C, 30.83; H, 3.46; N, 4.79. ^{1}H NMR (400 MHz, $CDCl_3$): 8.96 (4H, dmap-ortho), 7.23 (4H, dmap-meta), 3.31 (12H, dmap CH_3), 2.20 (12H, acetate CH_3), 2.10 (12H, acetate CH_3), 1.93 (12H, acetate CH_3) ppm. KBr (νCO): 1941 cm^{-1}. UV−vis: 612, 480, 408, 315, 258, 235 nm.

(ii) BL = 2-Methylpyrazine, 3. The same general procedure was followed as for **2**, with the exception of the purification step. After stirring overnight, the reaction mixture was filtered over a short plug of silica gel, and the product was eluted with a 2% MeOH in CH_2Cl_2 solution. The solvent was evaporated. The blue-green residue was redissolved in a minimum of CH_2Cl_2, and the product dimer was precipitated with hexanes. Typical yield was 50%. Anal. calcd for $Ru_6C_{45}H_{62}O_{28}N_6$: C, 31.04; H, 3.59; N, 4.83. Found: C, 30.61; H, 3.86; N, 4.45. ^{1}H NMR (400 MHz, $CDCl_3$): 9.09 (1H, pz), 9.03 (1H, pz), 8.94 (1H, pz), 8.89 (4H, dmap-ortho), 7.21 (4H, dmap-meta), 3.31 (12H, dmap CH_3), 3.23 (3H, pz-CH_3), 2.18 (12H, acetate CH_3), 2.09 (12H, acetate CH_3), 1.93 (12H, acetate CH_3) ppm. KBr (νCO): 1947 cm^{-1}. UV−vis: 606, 470, 408, 316, 260, 232 nm.

(iii) BL = 2,5-Dimethylpyrazine, 4. The same procedure was followed as for **3**. Typical yield was 40%. Anal. calcd for $Ru_6C_{46}H_{64}O_{28}N_6$: C, 31.47; H, 3.67; N, 4.79. Found: C, 30.49; H, 3.61; N, 4.34. ^{1}H NMR (400 MHz, $CDCl_3$): 9.05 (2H, pz), 8.89 (4H, dmap-ortho), 7.22 (4H, dmap-meta), 3.31 (12H, dmap CH_3), 2.18 (12H, acetate CH_3), 2.09 (12H, acetate CH_3), 1.97 (12H, acetate CH_3) ppm. KBr (νCO): 1943 cm^{-1}. UV−vis: 597, 400, 316, 261, 232 nm.

(9) Horng, M. L.; Gardecki, J. A.; Papazyan, A.; Maroncelli, M. *J. Phys. Chem.* **1995**, *99*, 17311−17337.

(10) Kido, H.; Nagino, H.; Ito, T. *Chem. Lett.* **1996**, 745−746.

2. [$Ru_3(\mu_3\text{-}O)(\mu\text{-}CH_3CO_2)_6(CO)(py)]_2(\mu\text{-}BL$). (i) BL = Pyrazine-$d_4$, 6. The complex was prepared by the same procedure as **2**. Typical yield was 70%. Anal. Calcd for $Ru_6C_{40}H_{46}D_4O_{28}N_4$: C, 29.20; H, 3.29; N, 3.41. Found: C, 27.99; H, 2.99; N, 3.02. ^{1}H NMR (400 MHz, $CDCl_3$): 8.95 (4H, py-ortho), 8.17 (2H, py-para), 8.05 (4H, py-meta), 2.26 (12H, acetate CH_3), 2.17 (12H, acetate CH_3), 2.01 (12H, acetate CH_3) ppm. KBr (νCO): 1946 cm^{-1}. UV−vis: 608, 473, 336, 243 nm.

(ii) BL = 2-Methylpyrazine, 7. The complex was prepared in the same way as for **2**, but chromatography resulted in breaking apart of the bridging ligand linkage. The dimer was purified by recrystallization from dichloromethane/ether. The solid was dissolved in a minimum amount of CH_2Cl_2, the solution was cooled with ice, and ether was added dropwise until crystals formed. Typical yield was 70%. Anal. calcd for $Ru_6C_{41}H_{52}O_{28}N_4$: C, 29.73; H, 3.23; N, 3.38. Found: C, 29.54; H, 3.24; N, 3.24. ^{1}H NMR (400 MHz, $CDCl_3$): 9.31 (1H, pz), 9.08 (1H, pz), 9.00 (1H, pz), 8.96 (4H, py-ortho), 8.94 (1H, pz), 8.15 (2H, py-para), 8.04 (4H, py-meta), 3.25 (3H, pz-CH_3), 2.25 (12H, acetate CH_3), 2.17 (12H, acetate CH_3), 2.05 (12H, acetate CH_3) ppm. KBr (νCO): 1949 cm^{-1}. UV−vis: 604, 450, 338, 242 nm.

(iii) BL = 2,5-Dimethylpyrazine, 8. The same procedure was followed as for **7**. Typical yield was 70%. Anal. calcd for $Ru_6C_{42}H_{54}O_{28}N_4$: C, 30.22; H, 3.26; N, 3.36. Found: C, 30.10; H, 3.33; N, 3.18. ^{1}H NMR (400 MHz, $CDCl_3$): 9.05 (2H, pz), 8.92 (4H, py-ortho), 8.15 (2H, py-para), 8.04 (4H, py-meta), 3.10 (6H, pz-CH_3), 2.25 (12H, acetate CH_3), 2.18 (12H, acetate CH_3), 2.01 (12H, acetate CH_3). KBr (νCO): 1950 cm^{-1}. UV−vis: 602, 424, 333, 237 nm.

(iv) BL = 2-Chloropyrazine, 9. The same procedure was followed as for **7** except that the solution was refluxed overnight. Typical yield was 40%. Anal. calcd for $Ru_6C_{40}H_{49}O_{28}N_4$: C, 28.67; H, 2.95; N, 3.34. Found: C, 31.40; H, 3.28; N, 3.78. ^{1}H NMR (400 MHz, $CDCl_3$): 9.07 (4H, py-ortho), 8.92 (1H, pz), 8.64 (1H, pz), 8.58 (1H, pz), 8.15 (2H, py-para), 8.01(4H, py-meta), 2.15 (12H, acetate CH_3), 2.09 (12H, acetate CH_3), 1.91 (12H, acetate CH_3). KBr (νCO): 1943 cm^{-1}. UV−vis: 588, 434, 420, 237 nm.

3. [$Ru_3(\mu_3\text{-}O)(\mu\text{-}CH_3CO_2)_6(CO)(cpy)]_2(\mu\text{-}BL$). (i) BL = Pyrazine-$d_4$, 11. The complex was prepared in the same way as **2**. Typical yield was 40%. Anal. calcd for $Ru_6C_{42}H_{44}D_4O_{28}N_6$: C, 29.76; H, 2.62; N, 4.96. Found: C, 30.58; H, 2.98; N, 4.80. ^{1}H NMR (400 MHz, $CDCl_3$): 8.73 (4H, cpy-ortho), 8.21 (4H, cpy-meta), 2.23 (12H, acetate CH_3), 2.16 (12H, acetate CH_3), 2.01 (12H, acetate CH_3). KBr (νCO): 1950 cm^{-1}. UV−vis: 610, 450, 258, 230 nm.

(ii) BL = 2-Methylpyrazine, 12. The same procedure was followed as for **7**, with the exception that the resulting solid was recrystallized from dichloromethane/hexane. Typical yield was 40%. Anal. calcd for $Ru_6C_{43}H_{50}O_{28}N_6$: C, 30.29; H, 2.96; N, 4.93. Found: C, 29.98; H, 3.01; N, 4.69. ^{1}H NMR (400 MHz, $CDCl_3$): 9.20 (1H, pz), 8.84 (1H, pz), 8.78 (1H, pz), 8.77 (4H, cpy-ortho), 8.20 (4H, cpy-meta), 3.20 (3H, pz-CH_3), 2.22 (12H, acetate CH_3), 2.16 (12H, acetate CH_3), 2.00 (12H, acetate CH_3). KBr (νCO): 1946 cm^{-1}. UV−vis: 610, 443, 260, 230 nm.

(iii) BL = 2,5-Dimethylpyrazine, 13. The same procedure was followed as for **12**. Typical yield was 40%. Anal. calcd for $Ru_6C_{44}H_{52}O_{28}N_6$: C, 30.74; H, 3.05; N, 4.89. Found: C, 29.25; H, 3.10; N, 4.32. ^{1}H NMR (400 MHz, $CDCl_3$): 8.91 (2H, pz), 8.77 (4H, cpy-ortho), 8.20 (4H, cpy-meta), 3.03 (6H, pz-CH_3), 2.22 (12H, acetate CH_3), 2.16 (12H, acetate CH_3), 2.00 (12H, acetate CH_3). KBr (νCO): 1943 cm^{-1}. UV−vis: 609, 429, 264, 231 nm.

Electrochemical Measurements. Cyclic voltammograms were measured with a BAS CV-50W Voltammetric Analyzer at a scan rate of 100 mV/s, using 0.1 M dichloromethane solutions of tetrabutylammonium hexafluorophosphate as electrolyte. All measurements were referenced to the ferrocene/ferrocenium potential.

Low-temperature spectroelectrochemical measurements were performed using an infrared reflectance cell described elsewhere.[11]

Low-temperature electronic spectroscopy was also carried out in the spectroelectrochemical cell described previously.[11] The measurements were performed in a Shimadzu UV-3101PC under a nitrogen atmosphere.

Calculation of Pyrazine Orbital Energies. Calculations were carried out with Mac GAMESS,[12] using the 6-31G basis set at the restricted Hartree−Fock level.

Results and Discussion

Synthesis and Characterization of [$Ru_3(\mu_3\text{-}O)(\mu\text{-}CH_3CO_2)_6(CO)(L)]_2(\mu\text{-}BL$). All compounds **1**−**13** were prepared by following a modification of previously reported "building block" strategies.[10] In the neutral state, each Ru_3 unit formally contains two Ru(III) and one Ru(II) centers with the CO ligand bound to a formally Ru(II) center.[13] Dimer stability is affected by the balance between the donor strengths of both ancillary and bridging ligands. It was previously noted that a more pronounced electron-donor character in ancillary ligands increases the energy of cluster-based dπ* orbitals, allowing for a more efficient overlap with bridging ligand-based π* orbitals.[4,5] Of course, it is also possible to alter the orbital energy overlap between dπ*(cluster) and π*(BL) by introducing substituents onto the pyrazine ring system. Bridging ligand substituents with electron-donor character increase the energy of π*(BL). Pyridine complexes **5**−**9** were obtained in good yields for all of the bridging ligands (BL = pz, d_4-pz mpz, dmpz, and clpz). Similar synthetic procedures for tetramethylpyrazine and phenazine did not yield dimeric species, probably due to combined effects of increased electron-donor character and steric hindrance, nor were dimers formed with dichloropyrazine as the bridging ligand. The compounds containing the strong donor dmap as ancillary ligand, **1**−**4**, were obtained in good yields that decrease with increasing steric bulk of the bridging ligand; i.e., yields increase in the order dmpz < mpz < pz = d_4-pz. Uniformly lower yields were obtained for the cpy series. Neither the dmap nor the cpy series formed dimeric species with chloro- or dichloropyrazine ligands.

Electronic Spectroscopy. All ruthenium clusters reported here show typical absorption spectral patterns in the UV−visible region. Assignments were made on the basis of previously reported compounds.[13−15] A broad band centered at ~605 nm is assigned to intracluster (Ru_3O) charge-transfer transitions (ICCT). This band is relatively insensitive to substitution of ancillary and bridging ligands and has been assigned to electronic transitions that arise from dπ(Ru)−p(O) mixing.[14] A second band, located at ca. 400−480 nm,

(11) Zavarine, I. S.; Kubiak, C. P. *J. Electroanal. Chem.* **2001**, *495*, 106−109.
(12) Schmidt, M. W.; Baldridge, K. K.; Boatz, J. A.; Elbert, S. T.; Gordon, M. S.; Jensen, J. H.; Koseki, S.; Matsunaga, N.; Nguyen, K. A.; Su, S. J.; Windus, T. L.; Dupuis, M.; Montgomery, J. A. *J. Comput. Chem.* **1993**, *14*, 1347−1363.
(13) Abe, M.; Sasaki, Y.; Yamada, Y.; Tsukahara, K.; Yano, S.; Yamaguchi, T.; Tominaga, M.; Taniguchi, I.; Ito, T. *Inorg. Chem.* **1996**, *35*, 6724−6734.

Table 1. UV−Visible Absorption Spectral Data for $[Ru_3(\mu_3\text{-}O)(\mu\text{-}CH_3CO_2)_6(CO)(L)]_2(\mu\text{-}BL)$

	L	BL	λ_{max}, nm (ϵ, $M^{-1}\,cm^{-1}$)
2	dmap	d_4-pz	235 (4.2×10^4); 258 (4.9×10^4); 315 (2.2×10^4); 408 (1.5×10^4); 480 (1.6×10^4); 612 (2.1×10^4)
3		mpz	232 (4.4×10^4); 260 (4.8×10^4); 316 (2.3×10^4); 408 (1.6×10^4); 470 (1.0×10^4); 606 (1.6×10^4)
4		dmpz	232 (3.0×10^4); 261 (3.5×10^4); 316 (1.8×10^4); 400 (1.1×10^4); 597 (1.0×10^4)
6	py	d_4-pz	243(3.5×10^4); 336 (9.8×10^3); 473 (1.2×10^4); 608 (1.4×10^4)
7		mpz	242(4.1×10^4); 338 (1.0×10^4); 450 (1.0×10^4); 604 (1.3×10^4)
8		dmpz	237(3.8×10^4); 333 (1.1×10^4); 424 (8.8×10^3); 602 (1.2×10^4)
9		clpz	237(3.9×10^4); 420 (9.6×10^3); 434 (9.6×10^3); 588 (8.8×10^3)
11	cpy	d_4-pz	230(3.5×10^4); 258 (1.5×10^4); 450 (1.1×10^4); 610 (9.0×10^3)
12		mpz	230(4.3×10^4); 260(2.9×10^4); 443(1.8×10^4); 610(1.5×10^4)
13		dmpz	231(4.7×10^4); 264 (3.2×10^4); 429 (1.9×10^4); 609 (1.4×10^4)

Table 2. Summary of Electronic Spectral Data for the Near-IR Bands of Mixed-Valence (−1) States of $[Ru_3(\mu_3\text{-}O)(\mu\text{-}CH_3CO_2)_6(CO)(py)]_2(\mu\text{-}BL)$[a]

BL	ν_{max} (cm^{-1})	ϵ_{max} ($M^{-1}\,cm^{-1}$)	ν_{max} (cm^{-1})	ϵ_{max} ($M^{-1}\,cm^{-1}$)
6 d_4-pz	11,100	19,000	7,100	17,000
7 mpz	9,100	15,000	7,200	22,000
8 dmpz	9,200	9,600	7,300	17,000
9 clpz	9,900	15,000	8,100	13,000

[a] Data were recorded in dichloromethane at −30 °C.

is assigned to cluster $\pi(Ru_3O)$ to ligand π^* transitions (CLCT).[13,15] This band is sensitive to the electron-donor character of L and BL and shifts to shorter wavelengths with increasing basicity of bridging ligands. Intense bands located ca. 235−338 nm are assigned to $\pi-\pi^*$ intraligand transitions. UV−visible spectral features for all compounds in dichloromethane are summarized in Table 1.

Electronic transitions were also examined for the singly reduced (mixed-valence) species of **6**−**9** in the near-infrared region. Previous reports noted that neutral Ru_3 systems do not display absorption bands in the near-IR states, whereas the mixed-valence (−1) states show two main absorption bands around 11 000 and 7000 cm^{-1}.[5] Similar near-IR absorptions are observed with substituted pyrazines as bridging ligands and are summarized in Table 2.

Recent results have underscored the utility of a three- or five-state vibronic coupling model to describe the spectroscopy of these mixed-valence compounds.[16−23] In particular, resonance Raman spectra (λ_{exc} = 752 and 801 nm) exhibited enhancement of several totally symmetric modes of the bridging pyrazine and ancillary pyridyl ligand,[18,19] and an infrared study of the mixed-valence state of three symmetric dimers found that the appearance and anomalous intensity of the *symmetric* (and formally IR forbidden) ν_{8a} mode of pz in the infrared spectrum of the mixed-valence state had vibronic origins.[24] This band did not appear in the spectra of the neutral or doubly reduced dimers nor in the spectra of the related cluster monomers, $[Ru_3O(\mu\text{-}OAc)_6(CO)(L)(L')]$, ruling out structural (electronic) symmetry breaking as a possible source of infrared enhancement. The conventional Marcus−Hush theory does not capture these observations. Instead, these complexes have been best explained in terms of a five-state vibronic coupling model.[20]

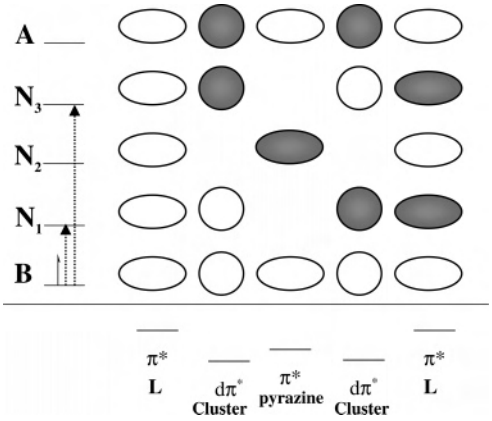

Figure 2. Molecular orbitals of a five-site vibronic coupling model for the ruthenium cluster dimers. The two symmetry-allowed transitions are B to N_1 and B to N_3.[20]

The vibronic coupling model first developed by Ondrechen et al.[21−23] (Figure 2) takes into account the electronic and vibrational participation of the bridging and ancillary ligands in addition to the metal clusters. The important interactions are the adjacent pairwise combinations of the five available electronic basis states: pyridyl ligand (1), metal cluster (1), bridging ligand, metal cluster (2), and pyridyl ligand (2) (Figure 2); the important molecular vibrations which are coupled to these electronic transitions are shown in Figure 3. The real distinction of this model from previous vibronic coupling models is that, in addition to explicitly including participation of the bridge, the importance of *symmetric* modes to the electron-transfer coordinate is highlighted. Full delocalization is not a requirement of this model; however, there must be strong exchange coupling interactions between adjacent sites.[22] (See ref 20 for a full description of the application of Ondrechen's model to these complexes.) It can be seen from Figure 2 that there are two symmetry-allowed transitions in this model. The transition that was previously described as cluster-to-cluster ("intervalence") charge transfer[5] (ca. 9000−11 000 cm^{-1}) is instead considered formally bridging ligand-to-ruthenium cluster charge transfer in character by the vibronic coupling model. This is

(14) Baumann, J. A.; Salmon, D. J.; Wilson, S. T.; Meyer, T. J.; Hatfield, W. E. *Inorg. Chem.* **1978**, *17*, 3342−3350.
(15) Baumann, J. A.; Wilson, S. T.; Salmon, D. J.; Hood, P. L.; Meyer, T. J. *J. Am. Chem. Soc.* **1979**, *101*, 2916−2920.
(16) Hush, N. *Prog. Inorg. Chem.* **1967**, *8*, 391−444.
(17) Sutin, N. *Prog. Inorg. Chem.* **1983**, *30*, 441−498.
(18) Londergan, C. H.; Rocha, R. C.; Brown, M. G.; Shreve, A. P.; Kubiak, C. P. *J. Am. Chem. Soc.* **2003**, *125*, 13912−13913.
(19) Rocha, R. C.; Brown, M. G.; Londergan, C. H.; Salsman, J. C.; Kubiak, C. P.; Shreve, A. P. *J. Phys. Chem A* **2005**, *109*, 9006−9012.
(20) Londergan, C. H.; Kubiak, C. P. *J. Phys. Chem A* **2003**, *107*, 9301−9311.
(21) Ondrechen, M. J.; Ko, J.; Zhang, L. T. *J. Am. Chem. Soc.* **1987**, *109*, 1672−1676.
(22) Zhang, L. T.; Ko, J.; Ondrechen, M. J. *J. Phys. Chem.* **1989**, *93*, 3030−3034.
(23) Ferretti, A.; Lami, A.; Ondrechen, M. J.; Villani, G. *J. Phys. Chem.* **1995**, *99*, 10484−10491.
(24) Londergan, C. H.; Salsman, J. C.; Ronco, S.; Kubiak, C. P. *Inorg. Chem.* **2003**, *42*, 926−928.

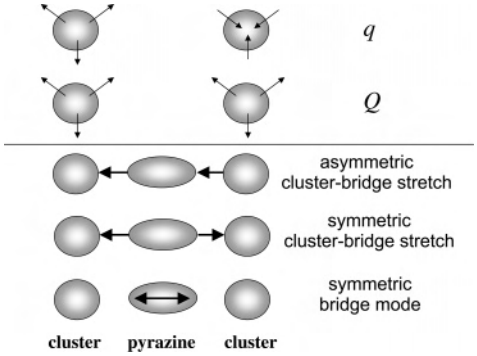

Figure 3. Molecular vibrations important for electron transfer in the three- (or five-) state model. *Q* and *q* are the symmetric and antisymmetric combinations of cluster breathing modes, respectively.

a B-to-N_3 transition, because this transition is from the ground state that has bridging ligand character to an excited state that does not. The low energy absorption (ca. 7000−8000 cm^{-1}) can be assigned similarly as B to N_1. In this way, two bands observed in the mixed-valence state can be considered transitions between two Hückel-type molecular orbitals over the entire complex rather than between two "metal ions." The relative ordering of the absorption energies observed for $\mathbf{6}^-$−$\mathbf{8}^-$ can then be understood in simple terms of the ground state (B) destabilization of the mpz- and dmpz-bridged dimers (**7** and **8**) relative to the d_4-pz-bridged dimer (**6**) due to the electron-donating nature of the methyl substituent(s) on the substituted bridges. This trend is further supported by the calculation of higher LUMO energies for mpz and dmpz relative to the other bridging ligands (Table 5). Importantly, the vibronic coupling model captures all of the trends in the low-energy intervalence charge-transfer region of the visible near-IR spectra of the mixed-valence (−1) state of all but one of the dimers reported here. The only exception is compound **9**, for which substantial physical evidence exists that it is a completely valence-trapped system (vide infra).

In this spectroscopic analysis, it appears that the clpz compound (**9**) must be considered separately from charge-transfer complexes **5**−**8** due to the high degree of electronic asymmetry imparted to the cluster by the clpz bridge. In the context of the vibronic coupling model, this asymmetry results in a strong interaction between clpz and metal cluster (1) and a weak interaction between clpz and metal cluster (2) (which will further inductively influence the interactions between pyridyl ligand (1)−metal cluster (1) and pyridyl ligand (2)−metal cluster (2)). Thus, we classify the mixed-valence state of **9** as valence trapped, with the charge localized on the half of the cluster with more favorable orbital overlap. Further strong experimental evidence for valence trapping of this complex is found in the infrared spectroelectrochemistry of the ν(CO) band (vide infra). The lower energy absorption (B to N_1) of the mixed-valence state of **9** is a higher-energy transition than those observed for $\mathbf{6}^-$−$\mathbf{8}^-$, indicative of ground-state stabilization of the B state relative to $\mathbf{6}^-$−$\mathbf{8}^-$ due to favorable overlapping on one side of the complex and destabilization of the N_1 state (due to electronic population of the orbitals with unfavorable overlapping). It might be expected that the B-to-N_3 transition would also be at a higher energy than $\mathbf{6}^-$−$\mathbf{8}^-$, but it is only higher than $\mathbf{7}^-$ and $\mathbf{8}^-$ and is slightly lower than $\mathbf{6}^-$. This may indicate that the electronic population of the N_3 state is dominated by orbitals with more favorable overlapping.

Table 3. Electrochemical Data for $[Ru_3(\mu_3\text{-O})(\mu\text{-CH}_3CO_2)_6(CO)(L)]_2(\mu\text{-BL})$[a]

	BL	L	$E_{1/2}(0/-1)$ (V)	$E_{1/2}(-1/-2)$ (V)	ΔE (mV)	K_c
1	pz	dmap	−1.216	−1.649	435	2.27×10^7
2	d_4-pz	dmap	−1.216	−1.649	435	2.27×10^7
3	mpz	dmap	−1.249	−1.605	355	1.01×10^6
4	dmpz	dmap	−1.291	−1.613	320	2.58×10^5
5	pz	py	−1.133	−1.507	380	2.67×10^6
6	d_4-pz	py	−1.133	−1.507	380	2.67×10^6
7	mpz	py	−1.169	−1.503	334	4.63×10^5
8	dmpz	py	−1.207	−1.492	285	5.44×10^4
9	clpz	py	−1.198	−1.438	240	1.39×10^4
10	pz	4-cpy	−1.058	−1.313	255	1.69×10^4
11	d_4-pz	4-cpy	−1.058	−1.313	255	1.69×10^4
12	mpz	4-cpy	−1.110	−1.310	200	2.41×10^3
13	dmpz	4-cpy	−1.150	−1.300	150	3.44×10^2

[a] In dichloromethane at 25 °C; 0.1 M tetra-*n*-butylammonium hexafluorophosphate supporting electrolyte; potentials referenced to ferrocene.

In conclusion, the five-state vibronic coupling model accounts for the UV−vis−NIR electronic spectra of the complexes that form strongly delocalized mixed-valence states. This model is not applicable in the valence-trapped complexes, such as $\mathbf{9}^-$.

Electrochemistry. All compounds in this study display rich electrochemistry much like the ruthenium cluster dimers previously reported by this laboratory in collaboration with Ito et al.[4,5] Cyclic voltammograms were measured in dichloromethane with tetra-*n*-butylammonium hexafluorophosphate (TBAH) as the electrolyte (Table 3). All dimers display four reversible processes, two two-electron oxidation waves, and two sequential one-electron reduction waves. The reversible reduction processes are assigned to $Ru_3^{III,III,II}$-BL-$Ru_3^{III,III,II}$/$Ru_3^{III,II,II}$-BL-$Ru^{III,III,II}$ (0/−1) and $Ru_3^{III,II,II}$-BL-$Ru_3^{III,III,II}$/$Ru_3^{III,II,II}$-BL-$Ru_3^{III,II,II}$ (−1/−2). The trend in cyclic voltammetry data is in agreement with the location of metal-to-ligand charge transfer (MLCT) electronic absorption bands. That is, the average of the reduction potentials $E_{1/2}(0/-1)$ and $E_{1/2}(-1/-2)$ becomes more positive, and MLCT bands shift to lower energies as the electron-donor nature of the bridging ligand decreases.

The splitting between the (0/−1) and (−1/−2) potentials, $\Delta E_{1/2}$, provides a direct measure of the thermodynamic stability of the (−1) state. This stability is imparted by electron exchange in the mixed-valence state and is related to a comproportionation constant, $K_c = \exp[\Delta E_{1/2}F/RT]$, for the following equilibrium:

$$Ru_3^{III,III,II}\text{-BL-}Ru_3^{III,III,II} + Ru_3^{III,II,II}\text{-BL-}Ru_3^{III,II,II} \overset{K_c}{\rightleftharpoons} 2Ru_3^{III,II,II}\text{-BL-}Ru_3^{III,III,II}$$

It was noted previously that K_c values depend strongly on the nature of ancillary (py, 4-cpy, and dmap) and bridging (pz and 4,4′-bpy) ligands.[4,5] For the series of compounds under investigation, K_c values fall 3 orders of magnitude

Table 4. Comparison of Reduction Potentials of the Dimers and Monomers with Pyridine Ancillary Ligands and Varying Bridging Ligand

L	BL (TL)[a]	$E_{1/2}(0/-1)$ (V) monomer	$E_{1/2}(0/-1)$ (V) dimer	difference (mV)
py	d_4-pz	−1.249	−1.133	116
py	mpz	−1.266	−1.169	97
py	dmpz	−1.294	−1.207	87
py	clpz	−1.247	−1.198	49

[a] Terminal ligand, in the case of the monomers.

Table 5. Calculated LUMO Energies of Pyrazine Ligands

BL	hartree	eV	cm^{-1}
pz	0.094	2.50	20600
dmpz	0.103	2.80	22600
mpz	0.100	2.72	21900
clpz	0.074	2.00	16200

when the ancillary ligand is changed from dmap to py to 4-cpy and the bridging ligand is unchanged.

The presence of bridging ligand substituents also has a pronounced effect on $\Delta E_{1/2}$ and K_c (Table 3). K_c and ΔE values fall 5 orders of magnitude and almost 300 mV, respectively, going from the most strongly coupled dimers (**1**, **2**) to the least strongly coupled dimer (**13**). The ability to fine-tune the dπ*(cluster) electronic levels by changing the electron-donor nature of L combined with the ability to adjust the π*(BL) orbitals by introducing substituents on to the pyrazine ring results in highly specific synthetic tuning of the electronic communication in these complexes, representing differences of 5 orders of magnitude in K_c values. Further evidence for the stability of the (−1) state of the dimer due to charge transfer is found by comparing the reduction potentials of the isolated cluster monomers with terminal (η^1) pyrazine-type ligands to the (0/−1) couple of dimers **6**−**9** (Table 4). In every case, the (0/−1) reduction potential of the dimer is positive of the reduction potential of the monomer, and the difference between the reduction potentials, $[E_{1/2}^{dimer}(0/-1) - E_{1/2}^{monomer}(0/-1)]$, scales with the electrochemical splitting of the (0/−1) and (−1/−2) potentials of the dimer, $\Delta E_{1/2}$ (Table 3), underscoring the assertion that the main source of electrochemical splitting is cluster-to-cluster electronic communication.

The unsymmetric complexes bridged by the unsymmetric bridging ligands clpz and mpz present additional levels of complexity. In the unsymmetrical mixed-valence complexes, the total electrochemical splitting, $\Delta E_{1/2}$, reflects both the electronic interactions typical of a strongly electronically coupled mixed-valence complex and the intrinsically different reduction potentials of the clusters bound to different nitrogen atoms of an unsymmetrical clpz or mpz ligand (Figure 4). In some cases, we find that a seemingly small perturbation in electronic symmetry can be so great as to lead to valence trapping. This is the case for clpz. In the case of mpz, the degree of symmetry breaking is reduced, and it is possible to observe an equilibrium population of the two possible charge distributions; i.e., in a localized picture, the charge may preferentially reside on the left or right side of the complex. Equilibrium constants for charge distributions of this type were measured via selective isotopic substitution of the CO ligand (vide infra).

IR Spectroelectrochemistry. The vibrational spectra of all complexes in their various redox states were obtained by using reflectance IR spectroelectrochemistry.[11] Controlled potentials were applied to prepare the singly (−1) and doubly (−2) reduced states of clusters **1**−**13** for IR spectroscopic observations. In the isolated neutral state, all complexes show a single ν(CO) band around 1938 cm^{-1}. Doubly reduced species give rise to a single ν(CO) band at approximately 1890 cm^{-1}, reflecting identical redox states at each cluster unit. Singly reduced complexes show a broad absorption band near the average energy of both bands for the neutral and doubly reduced states.[4−6] The degree of coalescence of the infrared absorption bands depends on the electronic communication between both ruthenium clusters. IR spectra for clusters $\mathbf{6}^-$−$\mathbf{9}^-$ in 0.1 M tetra-*n*-butylammonium hexafluorophosphate are shown in Figure 5. As the degree of electronic coupling reflected in electrochemical data decreases, two bands become resolved. Noncoalesced bands indicate the "stopped exchange" limit on the IR spectroscopy scale. Line shapes from IR spectroelectrochemistry can be used to estimate rate constants for the electron transfer using a Bloch-type analysis applied to infrared spectroscopy.[7] Calculated rate constants are in the picosecond regime (Table 6). As expected, k_{et} values follow the trend observed by electrochemical measurements of K_c and compare well with previously reported rate constants for similar compounds.[4,5,25]

Observation of "Mixed-Valence Isomers". Unlike the other complexes reported in this study, the asymmetrically bridged complexes $\mathbf{3}^-$, $\mathbf{7}^-$, $\mathbf{9}^-$, and $\mathbf{12}^-$ undergo electron

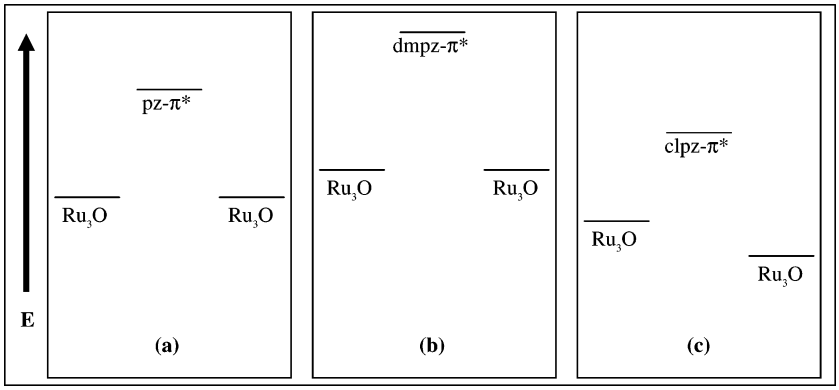

Figure 4. Qualitative molecular orbital scheme for the overlap of ruthenium clusters with bridging ligands: (a) pz, **5**, (b) dmpz, **8**, and (c) clpz, **9**.

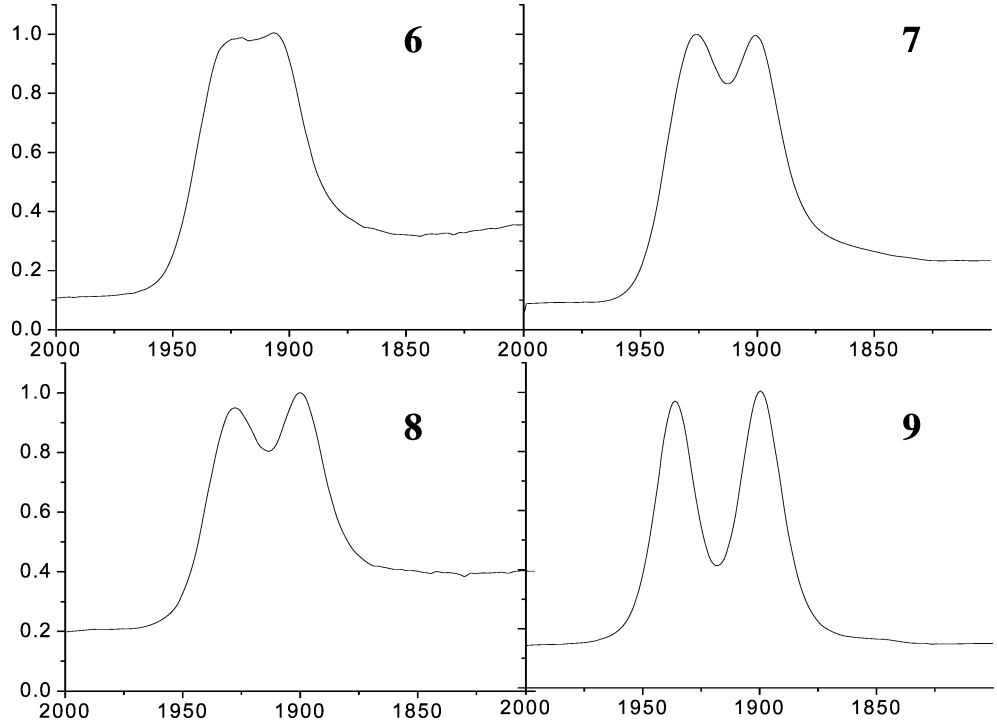

Figure 5. IR spectra for the mixed-valence states of $[Ru_3(\mu_3\text{-}O)(\mu\text{-}CH_3CO_2)_6(CO)(py)]_2(\mu\text{-BL})$ (**6**−**9**).

Table 6. Rate Constants for Electron Transfer

	L	BL	$k_{et}(s^{-1})$
1, **2**	dmap	pz, d_4-pz	2.0×10^{12}
4		dmpz	1.5×10^{12}
5, **6**	py	pz, d_4-pz	1.8×10^{12}
14, **15**		mpz[a]	1.2×10^{12}
8		dmpz	1.2×10^{12}
10, **11**	cpy	pz, d_4-pz	1.2×10^{12}
13		dmpz	7.0×10^{11}

[a] This is the "downhill" rate of electron transfer with a calculated $K_{eq} = 2.2$

transfer in the presence of a driving force. Determination of the equilibrium constant for the charge distribution introduced by this driving force by IR spectroscopy is not possible owing to essentially complete overlapping of the CO stretching frequencies for each mixed-valence isomer. Therefore, isotopic substitution of the CO ligand is required to spectroscopically differentiate the two sides of the mixed-valence complex. **14** and **15**, Figure 6, were synthesized as appropriate analogues to **7**.[26] The complexes were synthesized according to a modification of the synthesis described for **7** in which the precursor trinuclear cluster, $[Ru_3O(\mu\text{-}CH_3COO)_6(CO)(py)]$mpz, was synthesized as one regioisomer. The more basic nitrogen (α to the methyl group) is also the more sterically hindering to cluster ligation; thus, it is the less basic nitrogen that binds to the first ruthenium cluster under kinetic control. In a subsequent step, the second cluster is added and binds to the terminal pyrazine nitrogen. In this way, the two dimers were synthesized as pure materials starting with an unlabeled CO-substituted trinuclear cluster (**14**) or a $^{13}C^{18}O$-labeled cluster (**15**).

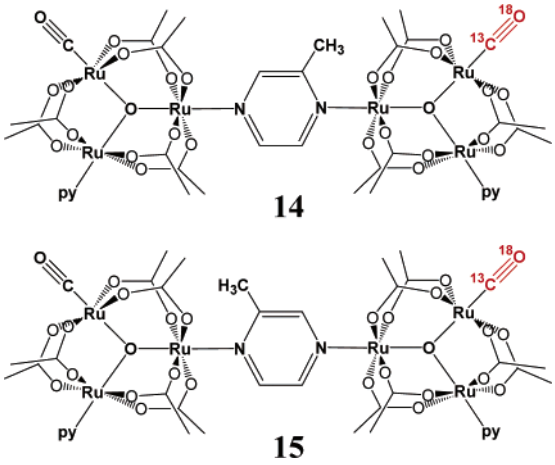

Figure 6. Structures of isotopically labeled dimers, differing only in position of the methyl group on the pyrazine bridge relative to the label.

Cyclic voltammetry of **14** and **15**, in a 0.1 M tetrabutylammonium hexafluorophosphate solution in methylene chloride vs the ferrocene/ferrocenium reference, reveals two two-electron oxidations ($E_{1/2} = 200$ and 1000 mV) and two one-electron reductions ($E_{1/2} = -1160$ and −1500 mV). The splitting in the reduction waves, $\Delta E_{1/2}$, is 340 mV and corresponds to a comproportionation equilibrium constant of 5.6×10^5. The total electrochemical splitting reflects both the electronic interactions typical of a strongly electronically coupled mixed-valence complex and the intrinsically different reduction potentials of the clusters bound to the different nitrogen atoms of the bridging methyl pyrazine ligand.[5,25] The equilibrium constant between the mixed-valence isomers formed from **14** and **15** are, in fact, small, and thus, the electrochemical splittings observed by cyclic voltammetry are dominated by the electronic interactions. This indicates the presence of a strongly coupled mixed-valence state.

(25) Ito, T.; Imai, N.; Yamaguchi, T.; Hamaguchi, T.; Londergan, C. H.; Kubiak, C. P. *Angew. Chem., Int. Ed.* **2004**, *43*, 1376−1381.
(26) Salsman, J. C.; Kubiak, C. P.; Ito, T. *J. Am. Chem. Soc.* **2005**, *127*, 2382−2383.

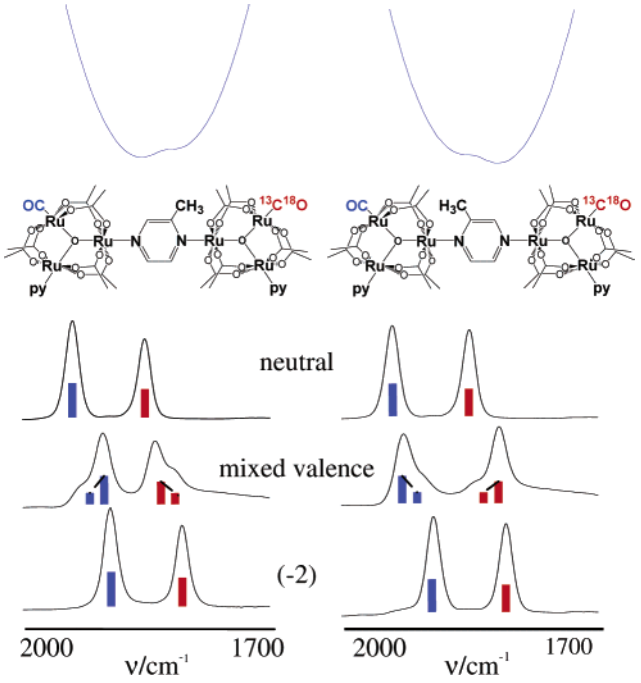

Figure 7. Infrared spectroelectrochemistry of **14** (left) and **15** (right) at −30 °C in a 0.1 M tetra-*n*-butylammonium hexafluorophospate solution in CH_2Cl_2. Spectra for the neutral (top), charge transfer (middle), and doubly reduced (bottom) states are shown with a schematic of the exchanging populations. Qualitative potential energy surfaces showing the double minima of the major and minor isomers are shown at top.

Infrared spectroelectrochemistry of **14** and **15** reveals exchange pairs consistent with mixed-valence isomerism (Figure 7). In the case of **14** (Figure 7, left), the neutral and doubly reduced (−2) states each show two ν(CO) bands separated by ca. 90 cm^{-1}, the intrinsic frequency separation due to the isotope substitution, $\nu(^{12}C^{16}O)$ vs $\nu(^{13}C^{18}O)$. In the mixed-valence (−1) state of **14**, *four* ν(CO) bands are observed, and these correspond (from higher to lower energy) to (1) the $\nu(^{12}C^{16}O)$ contribution from the minor (less stable) mixed-valence isomer, (2) the $\nu(^{12}C^{16}O)$ contribution from the major (more stable) mixed-valence isomer, (3) the $\nu(^{13}C^{18}O)$ contribution from the major isomer, and (4) the $\nu(^{13}C^{18}O)$ contribution from the minor isomer. Note that in the mixed-valence state of **14**, the spectral pattern (from higher to lower energy) corresponds to contributions from the minor, major, major, and minor isomers, whereas in the mixed-valence state of **15**, the spectral pattern is reversed to major, minor, minor, major. This is the expected result of reversing the side of the asymmetric mixed-valence complex that contains the $^{13}C^{18}O$ ligand. Because of the N-atom basicity differences of the mpz ligand, the minor isomer of **14** is expected to have the negative charge mostly on the cluster with the $^{13}C^{18}O$ ligand. The lowest frequency component of the overall ν(CO) spectrum is assigned easily to the cluster of the minor isomer bearing both the negative charge and the $^{13}C^{18}O$ because both the charge and heavier isotopes shift ν(CO) to a lower frequency. For similar reasons, the highest frequency part of the overall ν(CO) spectrum is assigned to the $^{12}C^{16}O$-substituted cluster of the minor isomer because ν(CO) will be unaffected by either charge or heavier isotope substitution. The remaining, more intense bands in the center of the ν(CO) spectrum of the mixed-valence state of **14** are assigned to the major isomer. Reversing the $^{13}C^{18}O$-substituted side of the cluster in going from **14** to **15** reverses whether each spectral component originates from the major or minor isomer. These data provide the most compelling evidence to date of the existence of mixed-valence isomers as discrete chemical species. It can also be seen that both the high frequency $\nu(^{12}C^{16}O)$ and low frequency $\nu(^{13}C^{18}O)$ portions of the IR spectra of the mixed-valence states are extensively coalesced exchange line shapes resulting from the dynamics of the intramolecular electron transfer between the minor and major mixed-valence isomers. Using the same line-shape simulation methods as for the symmetically substituted dimers, we can estimate the rate constants for electron exchange as well as the equilibrium constant between the major and minor mixed-valence isomers.

Analysis of the spectral line shapes of $\mathbf{14}^-$ and $\mathbf{15}^-$ gave an uphill rate for charge transfer of 6.5×10^{11} s^{-1} and an equilibrium constant of 2.2 for the charge distribution, which compares well with previously reported rate constants for similar mixed-valence dimers of trinuclear ruthenium clusters.[4,25]

9, which is also bridged by an unsymmetric bridging ligand (clpz), appears to be at the limit of valence trapping by infrared spectroelectrochemistry (Figure 5). The two peaks present in the (−1) state of the dimer are fully resolved and appear at the same frequencies as the single peaks observed in the spectra of the neutral and (−2) species. This suggests that the rate of electron transfer in this dimer can be no faster than 10^{11} s^{-1}. Therefore, the observed infrared spectrum is essentially that of one valence isomer, in stark contrast to the highly coupled complexes **14** and **15**.

Conclusions

We have shown that introducing substituents onto the pyrazine bridging ligand in dimers of ruthenium trinuclear clusters fundamentally affects the degree of intercluster electronic communication. The cyclic voltammetric and spectroelectrochemical data clearly show decreased coupling in cluster dimers with dimethyl-substituted pyrazine bridges. Using only three different ancillary ligands and four different bridging ligands, the comproportionation constants for the mixed-valence states relative to the neutral and (−2) states could be fine-tuned over 5 orders of magnitude. This demonstrates our explicit synthetic control over electronic coupling in dimers of ruthenium trinuclear clusters. Additionally, evidence for the presence of mixed-valence isomerism in the asymmetrically substituted 2-methyl- and 2-chloropyrazine bridges was found, and isotopic substitution of the CO ligand made it possible to determine rate and equilibrium constants for the charge distribution.

Acknowledgment. Financial support from NSF (CHE-0079182, an ROA supplement to this award to support S.R. as a visiting scientist, and CHE-0315593) is gratefully acknowledged.

IC050737V